Energy 244 (2022) 122563

Contents lists available at ScienceDirect

Energy

journal homepage: www.elsevier.com/locate/energy

Simplified model of battery energy-stored quasi-Z-source inverter-based photovoltaic power plant with Twofold energy management system

Lais de Oliveira-Assis [a], Emanuel P.P. Soares-Ramos [a, b], Raúl Sarrias-Mena [c], Pablo García-Triviño [a], Enrique González-Rivera [a], Higinio Sánchez-Sainz [d], Francisco Llorens-Iborra [a], Luis M. Fernández-Ramírez [a, *]

[a] Research Group in Sustainable and Renewable Electrical Technologies (PAIDI-TEP-023), Department of Electrical Engineering, University of Cadiz, EPS Algeciras, Avda. Ramón Puyol, S/n, 11202, Algeciras, Cadiz, Spain
[b] Federal Center for Technological Education of Minas Gerais, Department of Electro-electronics, R. Raymundo Matoso, 900, Santa Rita, Curvelo, MG, 35790-000, Brazil
[c] Research Group in Sustainable and Renewable Electrical Technologies (PAIDI-TEP-023), Department of Engineering in Automation, Electronics and Computer Architecture & Networks, University of Cadiz, EPS Algeciras, Avda. Ramón Puyol, S/n, 11202, Algeciras, Cadiz, Spain
[d] Research Group in Sustainable and Renewable Electrical Technologies (PAIDI-TEP-023), Department of Electrical Engineering, University of Cadiz, Department of Electrical Engineering, ESI Puerto Real, University of Cádiz, Avda. Universidad de Cádiz, N°10, 11519, Puerto Real, Cádiz, Spain

ARTICLE INFO

Article history:
Received 4 February 2021
Received in revised form
3 November 2021
Accepted 5 November 2021
Available online 9 November 2021

Keywords:
PV power Plant
Energy storage system
Quasi-Z-source inverter
Modelling
Control

ABSTRACT

The use of a battery energy-stored quasi-Z-source inverter (BES-qZSI) for large-scale PV power plants exhibits promising features due to the combination of qZSI and battery as energy storage system, such as single-stage power conversion (without additional DC/DC boost converter), improvements in the output waveform quality (due to the elimination of switching dead time), and continuous and smooth delivery of energy to the grid (through the battery energy storage system). This paper presents a new simplified model of a BES-qZSI to represent the converter dynamics with sufficient accuracy while using a less complex model than the detailed model (including the modelling of all switches and switching pulses). It is based on averaged values of the variables, voltage/current sources, and the same control circuit than the detailed model, except for the switching pulses generation. The simplified model enables faster time-domain simulation and is useful for control design and dynamic analysis purposes. Additionally, an energy management system has been developed to govern the power supply to grid under two possible scenarios: 1) System operator command following; or 2) economic dispatch of the stored energy. The results obtained from simulations and experimental hardware-in-the-loop (HIL) setup for different operating conditions of the grid-connected large-scale PV power plant with battery energy storage under study demonstrate the validity of the proposed simplified model to represent the dynamics of the converter and PV power plant for steady-state stability studies, long-term simulations, or large electric power systems.

© 2021 The Authors. Published by Elsevier Ltd. This is an open access article under the CC BY-NC-ND license (http://creativecommons.org/licenses/by-nc-nd/4.0/).

1. Introduction

Renewable energy systems (RES) are widely employed worldwide, and specifically photovoltaic (PV) systems are constantly expanding both in research as well as in industry/home applications. The energy generated by these PV systems needs to be converted before being delivered to the load or the grid. This conversion occurs typically in two stages. The first one is performed through a DC-DC converter, and in the second one, usually a voltage source inverter (VSI) allows the connection to the grid [1]. Typically, the DC-DC conversion stage boosts the voltage of the PV panels and implements the maximum power point tracking (MPPT) strategy of the PV generator, while the VSI is controlled to keep the voltage at

* Corresponding author.
E-mail addresses: lais.oassis@gmail.com (L. de Oliveira-Assis), emanuel@cefetmg.br (E.P.P. Soares-Ramos), raul.sarrias@uca.es (R. Sarrias-Mena), pablo.garcia@uca.es (P. García-Triviño), enrique.gonzalezrivera@uca.es (E. González-Rivera), higinio.sanchez@uca.es (H. Sánchez-Sainz), francisco.llorens@uca.es (F. Llorens-Iborra), luis.fernandez@uca.es (L.M. Fernández-Ramírez).

https://doi.org/10.1016/j.energy.2021.122563
0360-5442/© 2021 The Authors. Published by Elsevier Ltd. This is an open access article under the CC BY-NC-ND license (http://creativecommons.org/licenses/by-nc-nd/4.0/).

the DC link constant and regulate the reactive power exchange with the grid [2–4]. However, single-stage conversion is an attractive option due to its reduced losses, low device count and lower costs [5].

A large voltage boost in a single-stage can be achieved by Z-source inverters (ZSI), which include an impedance network before the VSI. Different topologies for ZSI can be found in Refs. [6,7]. A modified topology with a bi-directional power flow was proposed in Ref. [6]. An improved boost capability and a low voltage stress in the impedance source of a ZSI were analyzed in Ref. [7]. A derivation of ZSI is the quasi-Z-source inverter (qZSI), which presents differences in configuration, while maintaining the same operating principle. The benefits of the qZSI when compared to the ZSI are a lower component rating, no need for extra filtering capacitors, reduced switching ripples and constant DC input current from the PV panel [8].

PV systems with qZSI/ZSI for small-scale applications can be found in the literature [9–14]. An optimization based on a novel perturbation and observation algorithm was proposed in Ref. [9] to achieve the MPPT of a 4.5 kW PV system connected to grid through a qZSI. In Refs. [10–12], different modulation techniques were applied to ZSI/qZSI in small-scale PV system applications. A control strategy based on model predictive control was implemented for a three-phase qZSI in Ref. [13], while control loops with conventional PI controllers were used in Ref. [14].

Although RES present the advantages of vast fuel source and lower emissions of pollutants, their intermittent nature requires a special attention for their integration into the grid. If this integration is not dealt properly, excessive PV generation may lead to voltage instability, power fluctuation, or malfunctioning of the voltage regulation equipment, among other issues [15]. The use of energy storage systems with RES is an effective way to address the fluctuation and intermittency of the RES generation. A robust sizing of hybrid PV systems with battery is recommended when considering future variations of meteorological data and consumption profiles [16].

Among the existing large-scale energy storage technologies, batteries are widely employed [17,18]. Batteries can operate in charge or discharge mode according to the desired system operation. Most of the configurations with batteries and PV panels also include an additional DC-DC converter for the battery connection and a VSI for grid connection [19–21]. However, energy-stored qZSI represent a very interesting alternative for hybrid PV-battery systems without needing an additional DC/DC converter dedicated to the battery, since the battery is integrated into the impedance network of the qZSI in the energy-stored qZSI. This configuration allows an appropriate MPPT control of the PV panels, stable regulation of the DC voltage, and adjustable reactive power exchange through the control of the single inverter in the qZSI.

In the literature, qZSI have been used with energy storage systems in applications such as microgrids [22,23], induction motor for water pump [24], stand-alone wind turbines [25] and electric vehicles [26]. All these applications share the common objective of providing a stable power supply and enabling an efficient use of RES.

Some of the first applications of qZSI connected to small-scale PV systems and integrating energy storage systems can be seen in Refs. [8,27]. After these first applications, other research works with the same elements were also published, connecting the inverters in the cascaded multilevel topology [28], managing the battery state-of-charge (SOC) [29] or the power flow [30].

To guarantee a proper functioning of RES using battery energy storage, it is necessary to monitor and control the energy flow between sources and loads or grid [31]. This control is performed by an energy management system (EMS). In this work, the EMS must be able to achieve an appropriate balance between the PV system and the batteries. This will be done by ensuring a desired energy dispatch and controlling the battery SOC not to reduce its lifetime. In this context of design and evaluation of the control system and EMS, in which the details of high frequency components (such as the inverter switches) are not necessary, a simplified model for a battery energy-stored quasi-Z-source inverter (BES-qZSI) is proposed in this paper.

Two BES-qZSI models are considered in this work, the detailed model (DM) and the simplified model (SM). The DM includes the modelling of all switches and firing pulses, and is used as a benchmark to validate the results obtained with the proposed SM. The SM is based on averaged values of the variables, voltage/current sources and the same control circuit than the DM, except for the switching pulses generation. The main objective is to reproduce the response of the DM through the SM satisfactorily, while reducing the computational time and efforts significantly. This SM is suitable for long simulations, large-scale systems, control design and dynamic analysis purposes, where the switching features are not important.

Based on the premise that most of the BES-qZSI applications existing in the literature were reported for small-scale PV systems, the aim of this paper is to evaluate the performance of the SM for the BES-qZSI in a large-scale grid-connected PV system. In order to manage this PV power plant, an EMS is designed to control the battery charge and discharge depending on the PV generation, system operator (SO) demand, the electricity market, and the battery SOC. The proposed SM and EMS for the PV power plant are evaluated for different operating conditions: Changes in the solar irradiation, electricity market conditions and reactive power reference, as well as under a voltage sag as a grid disturbance. Furthermore, the adequate response of the SM compared to the DM has been validated with an experimental hardware-in-the-loop (HIL) setup. Therefore, the main contributions of this work can be summarized as follows: 1) Derivation of a simplified model for a BES-qZSI that reproduces the behavior of the detailed model adequately while reducing significantly the simulation time and computational efforts; 2) evaluation of the BES-qZSI simplified model in a large-scale PV system under different operating conditions; and 3) design of an EMS that can operate in two different scenarios to manage the power flow between the power sources and the grid.

In this work, the configuration of the PV power plant under study is described in Section 2. Section 3 illustrates the modelling and control of the DM and SM for the BES-qZSI. The EMS proposed for the PV power plant is explained in Section 4. Section 5 presents and discuss the results obtained. Finally, the concluding remarks are presented in Section 6.

2. Grid-connected PV power plant with BES-qZSI

The system under study is a grid-connected PV power plant composed by the PV panels, the BES-qZSI, an LCL filter, and a transformer. Fig. 1 shows the overall system with the control scheme implemented.

The rated power of the PV system is 172 kW, with nine modules connected in series and fifty-seven modules connected in parallel. SunPower SPR-X21-335-BLK PV modules [32] are used in this work.

The qZSI can boost the DC voltage and convert DC into AC in a single stage, making this converter a suitable option for the grid connection of RES with reduced cost. This converter also has the capacity to inject continuous input current and operates in the shoot-through state, avoiding the switching dead time needed in conventional VSI, thus enhancing the quality of the output signal [33]. The typical qZSI configuration is shown in Fig. 1. It is formed by

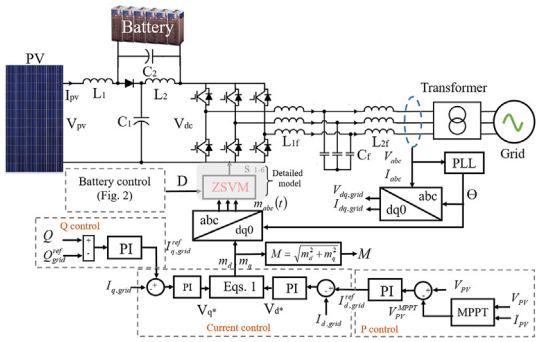

Fig. 1. Configuration and control scheme for the PV power plant with BES-qZSI.

a three-level VSI and an impedance network with two capacitors (C_1, C_2) and two inductors (L_1, L_2). These components are sized in order to limit the switching frequency of current and voltage [33]. The minimum value of the inductors can be calculated as follows.

$$L = L_1 = L_2 = \frac{T_{sh,max} M_{min} V_{in}}{2\, r_i I_{in}} \tag{1}$$

where r_i is the current ripple of the inductors (20%), $T_{sh,max}$ represents the maximum value of the shoot-through period (T_{sh}), $M_{\min}$ is the minimum value of modulation index (M), and I_{in} and V_{in} are the input current and voltage to the impedance network of the qZSI (I_{pv} and V_{pv}), respectively. $T_{sh,max}$ and $M_{\min}$ depend on the switching technique implemented, which is described in Section 3.1.

The minimum capacity of the capacitors is obtained through the following expression:

$$C = C_1 = C_2 = \frac{2 T_{sh,max} I_{in}}{r_v V_{dc}} \tag{2}$$

where r_v is the voltage ripple (1%), and V_{dc} is the DC voltage at the output of the impedance network.

The battery is connected in parallel with the capacitor C_2 of the qZSI and acts as a secondary energy source supporting the intermittent PV generation. A lead-acid battery with 18.75 kWh was used. This battery model presents a low cost, high reliability and high efficiency [17].

The LCL filter is the most suitable for large-scale RES applications [34]. The inductor (L_{1f}), capacitor (C_f) and inductor (L_{2f}) can be calculated through Eqs. (3)–(5), respectively.

$$L_{1f} = \frac{V_0}{2 \cdot \sqrt{6} \cdot f_s \cdot \Delta I_{L1f}} \tag{3}$$

$$C_f = X_f \cdot C_b \tag{4}$$

$$L_{2f} = r \cdot L_{1f} \tag{5}$$

where V_0 is the nominal line voltage, f_s is the switching frequency, ΔI_{L1f} is the maximum tolerable current ripple, X_f is the absorbed reactive power, C_b is the base capacitance and r is the ratio between L_{1f} and L_{2f}.

Detailed information about the sizing of the filter can be found in Ref. [35].

Finally, a 200 kW transformer with Y/Δ connection, 465 V/25 kV voltage ratio, and 60 Hz is used to connect the BES-qZSI to the grid. The transformer inductance and resistance parameters are $L_{pri} = L_{sec} = 0.001$ p. u, while $R_{pri} = R_{sec} = 0.03$ p. u. The magnetization inductance (L_{mag}) and resistance (R_{mag}) are 500 p. u.

Table 1 summarizes the most relevant parameters of the system under study.

Table 1
Summary of the system parameters.

PV panels		AC filter, transformer and grid	
$P_{pv\ rated}$	172 kW	f_{rated}	60 Hz
$V_{pv\ rated}$	515 V	$V_{grid\ rated}$	25 kV
		$V_{nom\ prim}$	465 V
Battery		$V_{nom\ sec}$	25 kV
Capacity	50 Ah	L_{prim}, L_{sec}	230 μH
$V_{b\ rated}$	375 V	R_{prim}, R_{sec}	23 mΩ
		L_{mag}	1H
qZSI		R_{mag}	377 Ω
$P_{qZSI\ rated}$	190 kW	Connection	Y/Δ
$V_{DC\ rated}$	900 V	L_{1f}	230 μH
L_1, L_2	79.5 μH	L_{2f}	8.6 μH
C_1, C_2	2200 μF	C_f	175 μF

3. Modelling and control of the battery ESS-qZSI

In this section, the modelling and control of the DM and SM for the BES-qZSI are explained.

3.1. Detailed model (DM) of the BES-qZSI: description and control

Fig. 1 shows the DM of the BES-qZSI, where all the components, including all switches and switching pulses, are modelled.

The control strategy implemented herein is depicted in Fig. 1. Maximum active power extraction from the PV system, reactive power and battery power control loops are shown in this figure. For the detailed model, an impedance-space-vector modulation technique (ZSVM) is applied. Therefore, the modulation index and the shoot-through duty cycle (namely M and D) are the terms that control the power flows in the system.

Many modulation techniques can be applied to qZSI. Simple boost control (SBC) maximum boost control (MBC), maximum constant boost control (MCBC) and ZSVM are the most significant. Regarding the ZSVM, several options appear depending on the switching pattern, such as ZSVM6, ZSVM4, ZSVM2 and ZSVM1. These techniques are described in Refs. [11,36]. In this work, ZSVM6 is used due to two main advantages compared to other techniques, such as a higher voltage gain and a lower voltage stress for the same voltage gain.

If the traditional SVM has six active states and two zero states, generating eight space vectors, the ZSVM adds one additional state, named the shoot-through state. In the ZSVM algorithm, the sample time (T_s) is divided into four periods (T_1, T_2, T_0 and T_{sh}). T_0, T_1 and T_2 are the time of application of the null, the first and the second active vectors respectively, and T_{sh} is the shoot-through period ($T_{sh} = DT_s$). For the ZSVM6, the switching times are calculated as follows:

$$\begin{cases} T_{\max+} = T_{\max} + \dfrac{T_{sh}}{12} \\ T_{\max-} = T_{\max} + \dfrac{T_{sh}}{4} \end{cases} \cdots \begin{cases} T_{mid+} = T_{mid} - \dfrac{T_{sh}}{12} \\ T_{mid-} = T_{mid} + \dfrac{T_{sh}}{12} \end{cases}$$

$$\begin{cases} T_{\min+} = T_{\min} - \dfrac{T_{sh}}{4} \\ T_{\min-} = T_{\min} - \dfrac{T_{sh}}{12} \end{cases} \tag{6}$$

The qZSI control is performed by controlling T_{sh} through D, and

by the modulation signals $m_a(t)$, $m_b(t)$ and $m_c(t)$. These last three terms represent a balanced three-phase signal. The module of these signals represented in the dq reference frame (m_d and m_q) corresponds to the modulation index M.

In Fig. 1, it can be observed that M is controlled to regulate the active power generated by the PV system, and the reactive power injected to the grid, through a cascaded control loop [37]. The inner loops are the current control loops, where two PI controllers regulate the d and q components of the grid current. These PI controllers generate u_d and u_q. Adding the corresponding decoupling terms, an independent regulation of active and reactive power can be accomplished through Eq. (7). The reference values for $i_{d,grid}$ and $i_{q,grid}$ are provided by the PI controllers in the outer control loop. One of these controllers is in charge of the active PV power generation, and the other one is in charge of the reactive power exchange with the grid. Once m_d and m_q are generated by Eq. (7), they are transformed to the abc reference frame to produce the IGBT firing pulses using ZSVM6.

$$\begin{aligned} m_d &= \frac{2}{V_{DC}}\left(u_d - L\cdot\omega_0\cdot i_{q,grid} + V_{d,grid}\right) \\ m_q &= \frac{2}{V_{DC}}\left(u_q - L\cdot\omega_0\cdot i_{d,grid} + V_{q,grid}\right) \end{aligned} \tag{7}$$

An MPPT strategy is necessary to benefit from the maximum solar radiance received by the PV modules. In the proposed configuration, a perturb and observe (P&O) algorithm was used, where the value of the maximum voltage is continuously tracked. The MPPT algorithm provides the reference voltage at the output of the PV panels (V_{pv}^{MPPT}), which is then compared with the voltage measured at the panels in the active power control loop.

On the other hand, the battery power exchange is regulated controlling the battery current (I_{ESS}) through D in the control loop shown in Fig. 2. In order to achieve a fast response, D is calculated as the sum of two terms ($D = \Delta D + D_0$). ΔD is the output of the battery current control loop, and D_0 is defined through Eq. (8), where V_{ESS}^{nom} is the nominal voltage of the energy storage system and V_{PV}^{std} is the input voltage of the qZSI at standard conditions of the PV system. Note that D_0 is constant. Therefore, ΔD makes D vary around D_0 to control the battery current.

$$D_0 = V_{ESS}^{nom} \Big/ \left(2\cdot V_{ESS}^{nom} + V_{PV}^{std}\right) \tag{8}$$

The active power reference for the battery P_{ESS}^{ref} is provided by the EMS. This value is then divided by the measured battery voltage V_{ESS} to obtain the current reference I_{ESS}^{ref}, as illustrated in Fig. 2. Due to technical constraints of the device, the battery current must remain between maximum and minimum values. Therefore, a saturation is imposed to I_{ESS}^{ref} previously to the comparison against the measured current I_{ESS}. The deviation between the actual and the desired battery current is inputted to a PI controller that generates ΔD as an output. Finally, D is computed adding D_0 to ΔD. In the detailed model, D is inputted to the ZSVM algorithm to implement the shoot-through states in the converter. On the other hand, the simplified model requires the calculation of the battery voltage V_{ESS}^{out} for the controlled voltage source that represents the battery in the averaged model of the converter. This voltage is calculated through Eq. (16), as it will be shown in Section 3.2, and this is the equation implemented at the rightmost part of Fig. 2.

3.2. Simplified model (SM) of the BES-qZSI: description and control

The SM of the qZSI replaces the impedance network and the VSI switches with controlled sources governed by the boost factor (B) and the modulation signals $m_a(t)$, $m_b(t)$ and $m_c(t)$. Because the firing

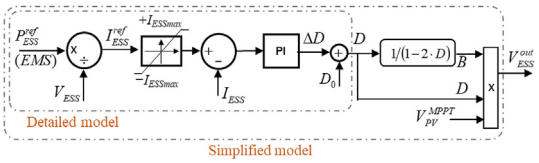

Fig. 2. Energy storage system power control.

pulses of the switches are not considered, the data processing needs are reduced notably (the sample time can be increased), while obtaining a performance similar to the DM. Thus, the proposed model does not show the current and voltage harmonics but the dynamic performance of the DM, which results important when it comes to manage the power flow.

The proposed SM is composed of a controlled current source in the PV system side, three controlled voltage sources in the grid side and a controlled voltage source that simulates the terminals of the capacitor C_2. Like in the DM, the battery is connected to this capacitor. Fig. 3 illustrates a scheme of the SM proposed for the BES-qZSI.

Considering ZSVM6 in the qZSI, the following two expressions relate the different voltages in the qZSI (i.e., V_{in}, V_{dc}, and V_{ac}).

$$V_{dc} = V_{in}\frac{1}{1-2D} \tag{9}$$

$$\begin{aligned} v_a(t) &= \frac{1}{\sqrt{3}}\left(V_{dc}\cdot m_a(t)\right) \\ v_b(t) &= \frac{1}{\sqrt{3}}\left(V_{dc}\cdot m_b(t)\right) \\ v_c(t) &= \frac{1}{\sqrt{3}}\left(V_{dc}\cdot m_c(t)\right) \end{aligned} \tag{10}$$

If V_{dc} is replaced in Eq. (10) using Eq. (9), a direct relationship between the AC output voltage of the converter and the input voltage V_{in} appears in Eq. (11).

$$\begin{aligned} v_a(t) &= B\cdot\frac{2}{3}V_{in}\cdot m_a(t) \\ v_b(t) &= B\cdot\frac{2}{3}V_{in}\cdot m_b(t) \\ v_c(t) &= B\cdot\frac{2}{3}V_{in}\cdot m_c(t) \end{aligned} \tag{11}$$

Since $m_a(t)$, $m_b(t)$ and $m_c(t)$ constitute a balanced three-phase signal, so is the aggregation of $v_a(t)$, $v_b(t)$ and $v_c(t)$. This can be achieved using the same control loops as in the DM.

In the DC side of the qZSI (PV system terminals), the value of the controlled current source is calculated based on the power balance principle ($P_{grid} = P_{PV} + P_{ESS}$) derived from the PV system side terminals (V_{in}).

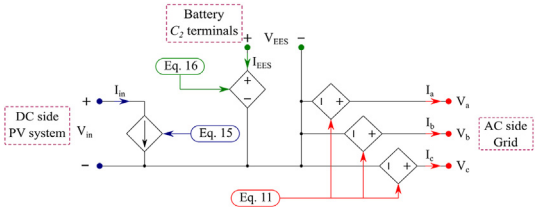

Fig. 3. Proposed simplified model.

$$\begin{aligned} P_{grid} &= i_a(t)\cdot v_a(t) + i_b(t)\cdot v_b(t) + i_c(t)\cdot v_c(t) \\ P_{in} &= V_{in}\cdot I_{in} \\ P_{ESS} &= V_{C2}\cdot I_{ESS} = V_{ESS}\cdot I_{ESS} \end{aligned} \tag{12}$$

Eq. (12) taken to the PV system side becomes Eq. (13). Note that V_{ESS} is equivalent to $V_{in}{\cdot}B{\cdot}D$.

$$\begin{aligned} P_{grid} &= \frac{V_{in}}{\sqrt{3}}\cdot B\cdot (i_a(t)\cdot m_a(t) + i_b(t)\cdot m_b(t) + i_c(t)\cdot m_c(t)) \\ P_{in} &= V_{in}\cdot I_{in} \\ P_{ESS} &= V_{in}\cdot B\cdot D\cdot I_{ESS} \end{aligned} \tag{13}$$

Finally, the input current can be calculated through the power balance.

$$\begin{aligned} &I_{in} = \frac{1}{\sqrt{3}}\cdot B\cdot (i_a(t)\cdot m_a(t) + i_b(t)\cdot m_b(t) + i_c(t)\cdot m_c(t)) - B\cdot D\cdot I_{ESS} \\ &i_a(t)\cdot m_a(t) + i_b(t)\cdot m_b(t) + i_c(t)\cdot m_c(t) \rightarrow m_{abc}(t)\cdot i_{abc}(t) \end{aligned} \tag{14}$$

$$I_{in} = \frac{1}{\sqrt{3}}\cdot B\cdot m_{abc}(t)\cdot i_{abc}(t) - B\cdot D\cdot I_{ESS} \tag{15}$$

where, $i_{abc}(t)$ is the current at the AC side, I_{ESS} is the energy storage system current and I_{in} is the current generated by the PV system.

Finally, as commented above, the energy storage is connected to a controlled voltage source that simulates the terminals of the capacitor C_2.

$$V_{ESS}^{out} = V_{PV}\cdot D\cdot B \tag{16}$$

In this model, the control loops for the output power of the PV system and the reactive power exchange with the grid are the same as in the DM, shown in Fig. 1. Furthermore, since the firing pulses of the VSI switches are not considered, M is calculated as the module of the vectors md and mq. Additionally, the battery control loop also has to generate proper values of D in order to control the energy storage system reference power provided by the EMS. In this case, once D is obtained, Eq. (16) is used to calculate V_{ESS}^{out}.

4. Energy management system

This section describes the EMS implemented to control the power flow between the energy sources, i.e. the PV system and the battery, and the grid (namely P_{PV}, P_b and P_{grid} respectively). A flowchart of the proposed EMS is shown in Fig. 4.

In a first stage, the EMS awaits for instructions of the SO. The top priority of the EMS is to comply with the active and reactive power requirements of the SO (P_{SO} and Q_{SO}) as long as they remain between certain boundaries. If the SO does not set any operating instructions, then the system is operated to make an economic profit of the energy stored following a simple scheme. These two possibilities are described in detail below.

In order to fulfill the SO requirements, P_{SO} must remain between the maximum and minimum available power (P_{av}^{max} and P_{av}^{min}) given by Eqs. (17) and (18) respectively. These boundaries are defined based on the maximum charge and discharge power of the battery ($P_b^{ch,max}$ and $P_b^{dis,max}$ respectively) according to Eqs. (19) and (20), which are computed considering the maximum and minimum SOC advised for the battery [38]. In this work, $SOC_{max} = 90\%$ and $SOC_{min} = 30\%$. This scheme protects the battery against overcharge and deep discharge. Additionally, the reactive power command Q_{SO} is limited by P_{SO} and the rated power of the converter. If both P_{SO} and Q_{SO} are set within the aforementioned limits, they become the active and reactive power references for the EMS ($P_{grid}^{ref} = P_{SO}$ and $Q_{grid}^{ref} = Q_{SO}$). Therefore, the SO must be informed of P_{av}^{max} and P_{av}^{min} to make a sensible selection of P_{SO} and Q_{SO}.

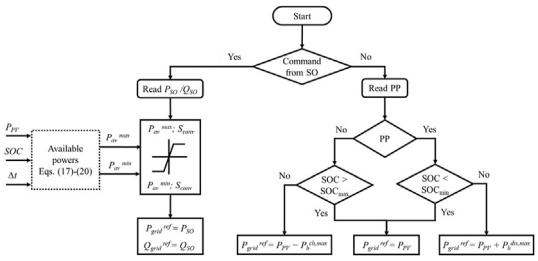

Fig. 4. Control scheme for the EMS.

$$P_{av}^{max} = P_{PV} + P_b^{dis,max} \tag{17}$$

$$P_{av}^{min} = P_{PV} - P_b^{ch,max} \tag{18}$$

$$P_b^{dis,max} = \min\left(P_b^{max},\ \frac{E_{bat}}{\Delta t}\left(\frac{SOC - SOC_{min}}{100}\right)\right) \tag{19}$$

$$P_b^{ch,max} = \min\left(P_b^{max},\ \frac{E_{bat}}{\Delta t}\left(\frac{SOC_{max} - SOC}{100}\right)\right) \tag{20}$$

where E_{bat} is the nominal energy of the battery, Δt is the time interval of the demanded energy, and P_b^{max} is the maximum power of the battery.

When no specific command is received from the SO, the battery is operated under economic profitability criteria. Because this paper does not focus on the detailed regulation of power generation in a complex electricity market, the EMS only discerns between valley periods (VP) and peak periods (PP). Nonetheless, the battery SOC limits still apply on this situation. In this sense, the EMS will charge the battery with $P_b^{ch,max}$ during VP only if $SOC < SOC_{max}$. On the other hand, the EMS will discharge the battery with $P_b^{dis,max}$ during PP if $SOC > SOC_{min}$. Storing energy in VP and releasing during PP increases the monetary profit of the hybrid system. However, if any of the SOC limits are reached either in VP or PP, the battery stops charging/discharging and only the PV generation is delivered to the grid ($P_{grid}^{ref} = P_{PV}$).

In the EMS proposed, P_{PV}, SOC, P_{SO}, Q_{SO} are used as inputs. Additionally, a binary variable PP is used to discriminate between PP (PP = 1) and VP (PP = 0) in the electricity market. Finally, P_{grid}^{ref} and Q_{grid}^{ref} are outputted from the EMS in any of the two scenarios considered: 1) SO command following; or 2) economic dispatch of the stored energy.

5. Results and discussion

In this section, the dynamic performance of the proposed SM and the DM of the BES-qZSI is evaluated and compared under changes in the solar irradiation, electricity market conditions and reactive power reference, as well as under a voltage sag as a grid disturbance. For comparison purposes, a third model has been included in this section. It has been labelled as 'mixed model' (MM), and it consists of the complete impedance network of the qZSI

implemented element by element as in the DM, and an averaged representation of the battery and the VSI using controlled sources as in the SM. In addition, the behavior of the proposed SM is studied for long simulations with different operating conditions on PV generation, battery and grid (changes in the electricity market and the power demanded by the SO). Moreover, an experimental HIL validation of the proposed SM is presented in this section. Finally, the execution time of the simulations is registered and compared to verify the computational requirements of each model.

5.1. Case 1: long simulation with changes in the solar irradiation and electricity market

In this case, a 30 s-long simulation is carried out to evaluate the performance of the models with changes in the solar irradiation and the electricity market.

Fig. 5 shows the irradiation profile used in this case, which represents the irradiation of a typical cloudy summer day, but compressed in 30 s of simulation. This irradiation profile allows to evaluate the behavior of the system with changes in the PV power, and thus, in the management of the power stored in/provided by the battery (P_b) and the power injected to the grid (P_{grid}). The simulation is performed assuming an initial battery SOC of 50%. The MPPT algorithm allows the PV array to operate with the maximum power at every instant.

It can be seen in Fig. 6a–c that the proposed SM achieves the expected objective, as the results obtained with the SM for the active power flows (P_{PV}, P_b and P_{grid}) are similar to those shown by the DM. Additionally, the MM used to reinforce the comparison presents a similar response to the SM, which indicates that the SM reproduces the DC dynamics of the qZSI satisfactorily. Moreover, since both the SM and the MM resemble the DM, it can be stated that the loss of information when using an averaged model of the VSI does not pose a significant drawback in this sort of simulations, since only the high switching frequency of the switches in the DM is obviated in the SM and MM, while reducing the simulation time and computational efforts notably.

In this simulation, the SO does not define any reference power. Therefore, the battery operates searching an economic benefit in the electricity market. Subsequently, during the VP (indicated with the red background in Fig. 6d) the energy is stored in the battery. The energy stored is released later during the PP (green background), making a monetary profit due to the difference in the energy cost between both periods.

5.2. Case 2: short simulation with changes in the reactive power reference and a grid disturbance

This simulation focuses on evaluating the proposed SM and the

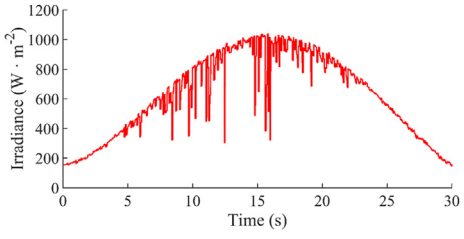

Fig. 5. Irradiation profile for case 1.

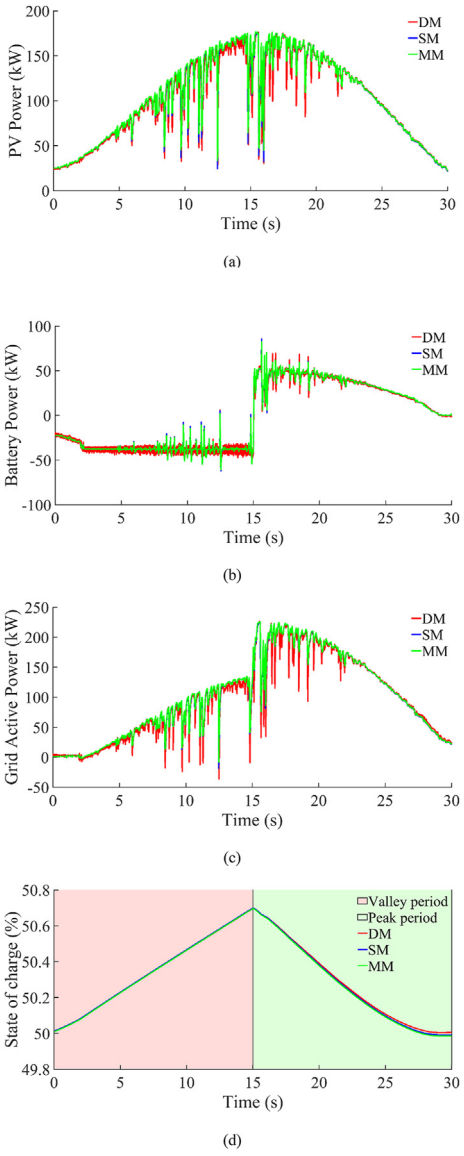

Fig. 6. Case 1: (a) PV power; (b) Battery power; (c) Grid power; and (d) SOC.

control system under transient states that may occur in the system, such as changes in the reactive power reference imposed by the SO and a grid disturbance (grid voltage sag of 0.7 p. u. at 2.5 s with a duration of 50 ms).

Fig. 7 illustrates the grid active and reactive power obtained in this case study, where the system is simulated under the following operating conditions: 1) the irradiation is assumed constant at 1000 W/m^2; b) the SO demands a P_{SO} of 190 kW, where the PV system contributes with 171 kW and the battery with 19 kW; 3) the system operates with unity power factor (reactive power equals to zero), excepting from 1 to 2 s, where the SO demands a Q_{SO} of −0.1 p. u. (equivalent to −20 kVAr), and from 3 to 4 s, where +0.1 p. u. (+20 kVAr) are requested.

Regarding the voltage sag, the system operates with an active power of 190 kW and unity power factor right before the disturbance. During the voltage sag, the active power falls equally in the three models (DM, SM and MM) due to the voltage drop. When the

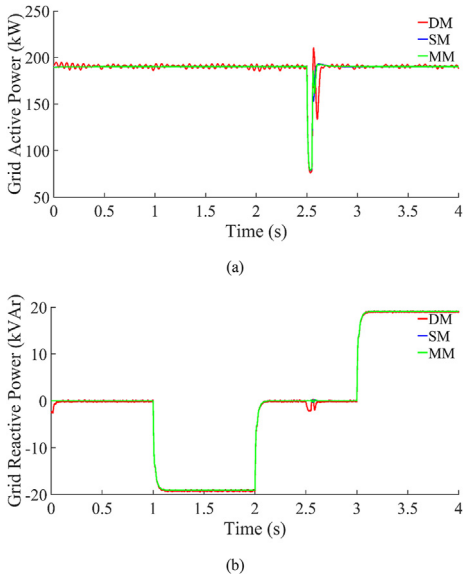

Fig. 7. Case 2: (a) Grid active power; and (b) Grid reactive power.

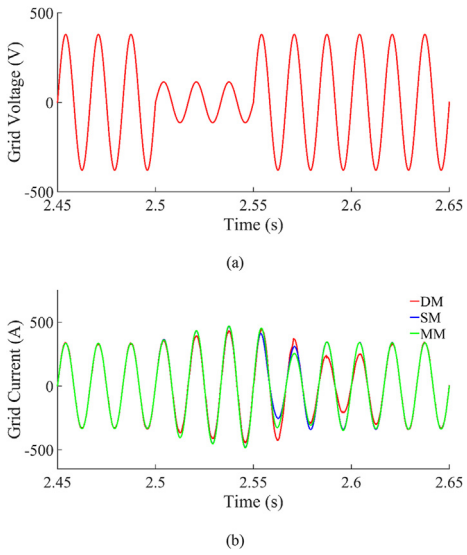

Fig. 8. Case 2: (a) Phase-A grid voltage; and (b) Phase-A grid current during the voltage sag.

disturbance is cleared and the grid voltage recovered, the active power increases and stabilizes at the pre-fault value. The SM and MM present less variability in the transient and reaches the pre-fault conditions earlier than the DM, provided that the operation of the power switches in the VSI is only considered in the latter. During the rest of the simulation, the results obtained by the proposed SM perfectly match with those achieved by DM and the MM, even when the changes in the reactive power happen.

Fig. 8 illustrates the effect of the voltage sag on the phase-A grid voltage and current. Since the grid is modelled as an ideal source, as illustrated in Fig. 1, only a single voltage waveform is represented in Fig. 8a, because it is exactly the same in the three models compared. Regarding the grid current in Fig. 8b, only small differences between the DM, the SM and the MM appear during and after the fault. It can be seen that the transitory state in the grid current observed for the DM is slightly more accused than the SM and the MM due to the simplifications made in these models. Nevertheless, the response of the SM and the MM is completely valid for the target simulations of these models, and they should only be discarded if a very detailed study of the fault dynamics was required, which is not the case in this work. Finally, the stabilization of the grid current after the fault indicates that the PV power plant and the battery are controlled satisfactorily once the grid voltage is recovered.

5.3. Case 3: experimental HIL validation

This section presents the experimental results that allow testing and comparing the real-time performance of the DM and the proposed SM.

Fig. 9 presents the experimental HIL setup built for the validation of the simulation results. The power plant runs in real-time in a *Typhoon HIL402* device. This real-time machine is programmed through the software *Typhoon HIL Control Center*, which also allows monitoring the most relevant parameters of the power system in real-time. The control system runs in a *dSPACE MicroLabBox*, programmed using Simulink, and using *dSPACE ControlDesk* to monitor the signals of interest. Finally, the figures presented in this section are obtained through a *Yokogawa DLM4038* oscilloscope that measures the inputs and outputs of both real-time simulators.

As it can be observed in Figs. 10 and 11, the results obtained with the experimental setup reveal that the proposed SM responds similarly to the DM under different operating conditions. In this sense, Fig. 10a shows that the DM tracks the references for the active and reactive powers satisfactorily, as well as the battery current. This indicates a proper operation of the control systems implemented. Additionally, the PV power generation and the battery power are also represented in this figure. The former varies with the irradiation input, and the latter is calculated from the battery voltage and current outputs. Fig. 10b illustrates an analogous scenario for the SM. As seen, the SM responds similarly to the DM under changes in the active and reactive powers, and the battery current, and no relevant differences can be highlighted.

Fig. 11 depicts the results of the experimental setup during a sag in the grid voltage of 0.7 p. u, during 50 ms. The grid active and reactive powers, plus the phase-A instantaneous voltage and current are represented for the DM and the SM (Fig. 11a and b, respectively). Even under this grid fault, both the DM and the SM are able to recover the control of the power system shortly after the fault clearance. Furthermore, similar results for the DM and the SM can be noticed when comparing Fig. 11a and b.

The experimental results shown in this section prove the adequacy of the SM to replace the DM in long-term simulations, large-scale electric power systems, and control design and dynamic analysis purposes.

5.4. Case 4: long simulation with changes in PV power, electricity market and power demanded by the SO

The results of an 8100 s-long simulation (equivalent to 2 h and 15 min) are presented in this section. Since the performance of the proposed SM has proved similar to the DM in the previous case, only the SM is simulated in this scenario to confirm its suitability for dynamic analysis purposes in long-term simulations. For this simulation, a variable irradiance profile following the P_{PV} pattern shown in Fig. 12a and different operating conditions of the electricity market (Fig. 12b) are considered. This allows to evaluate the PV power plant and the proposed EMS under all the operating

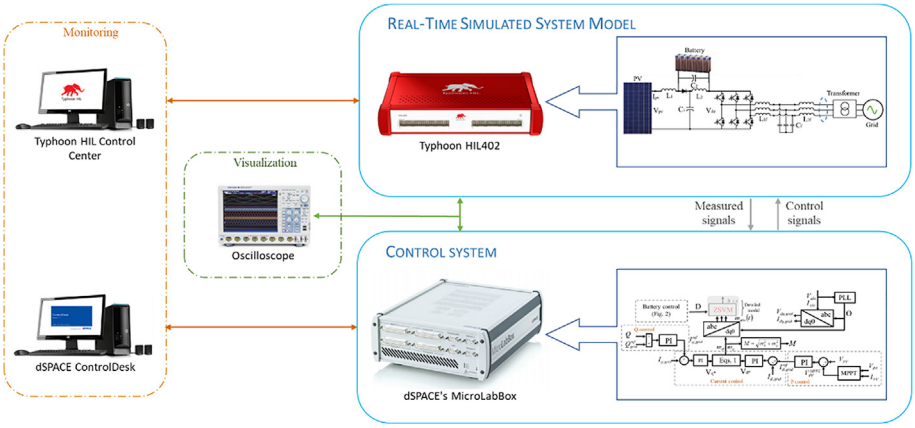

Fig. 9. HIL experimental setup.

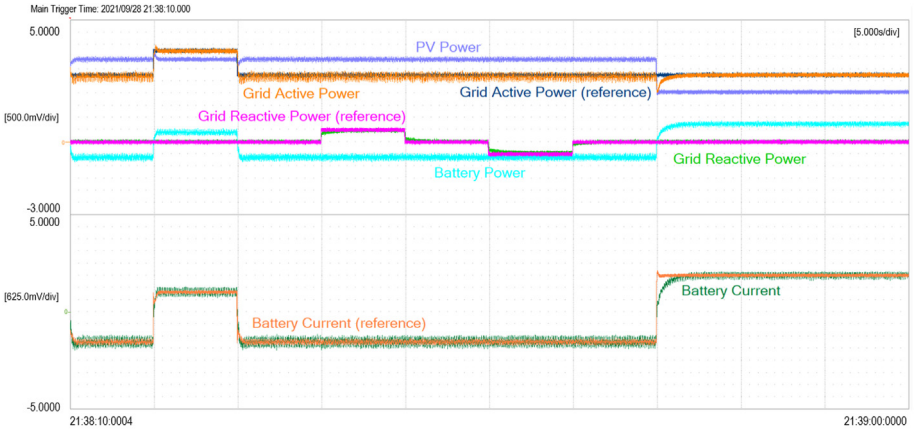

(a)

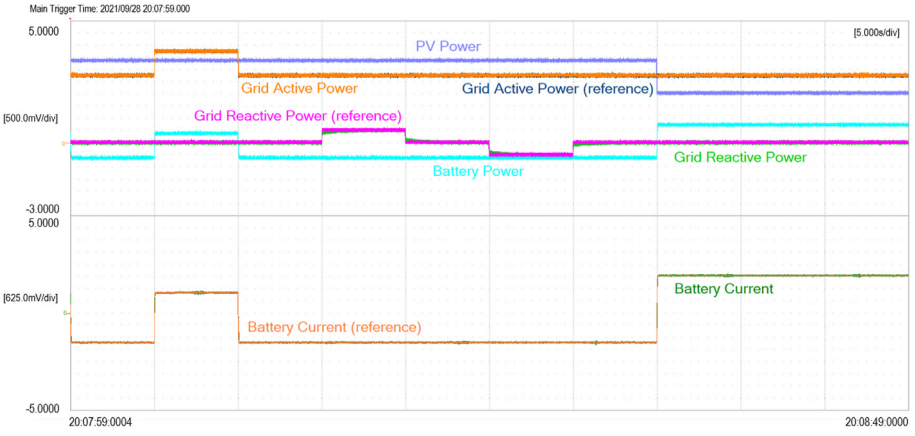

(b)

Fig. 10. Experimental results with power variation and battery current control for (a) Detailed model; and (b) Simplified model.

conditions described in Section 3 and Fig. 4.

Fig. 12a shows the power balance during the simulation for an initial SOC of 60% in the battery. It also presents the power demanded by the grid and the maximum available power. It can be noted from Fig. 12a that the demanded power is always lower than the maximum available power, and that when the SO demands a specific power, this request is addressed. From 0 to 1800 s, the SO defines a power demand. When the power requested by the SO is

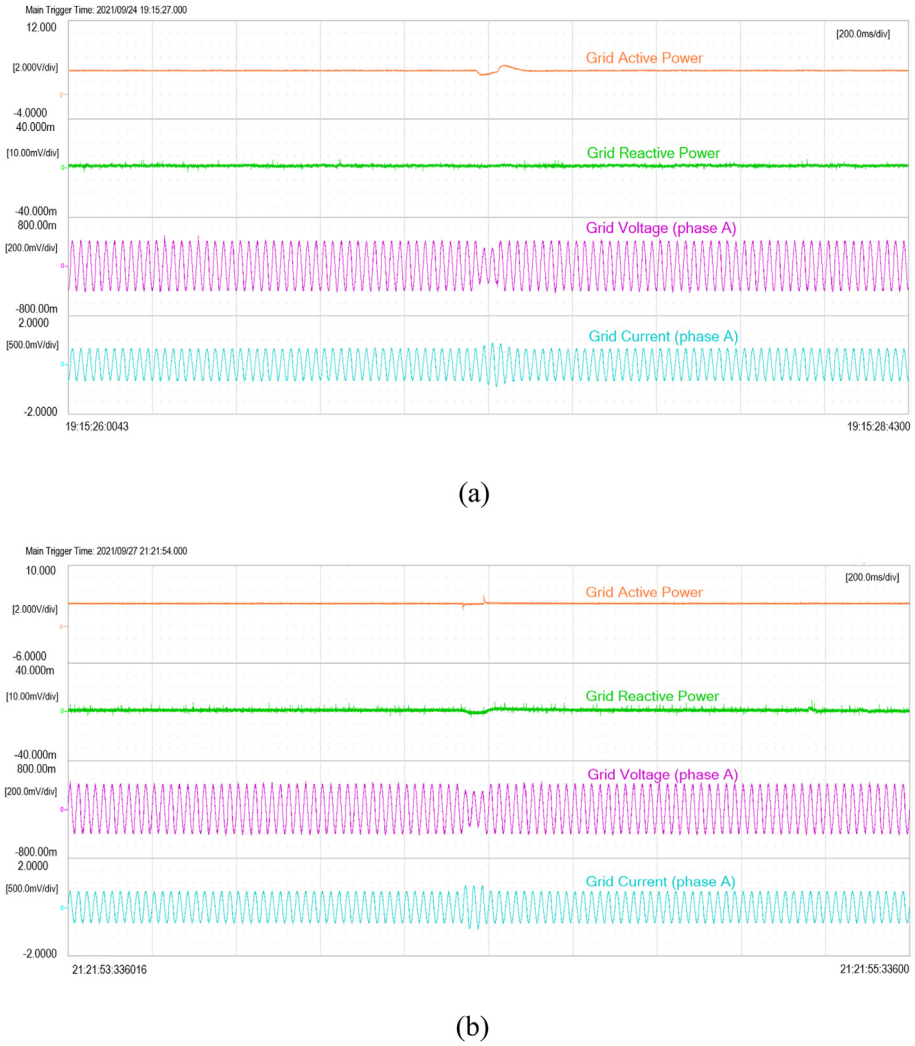

Fig. 11. Experimental results including a voltage sag for (a) Detailed model; and (b) Simplified model.

lower than the power generated by the PV panels, the exceeding energy is used to charge the battery. When the SO requests more power than the PV generation, the battery is discharged. From 1800 to 3600 s, the SO does not define any power demand, and the battery operates to achieve an economic benefit in the electricity market. In the first part of this period (from 1800 to 2700 s), the market is not favorable to sell energy (VP in Fig. 12b). Hence, the excess energy is stored in the batteries. On the other hand, in the second part (from 2700 to 3600 s) a PP is observed (Fig. 12b), and thus the battery is discharged. Approximately at the middle of the peak period, the battery is discharged with a lower intensity, limited by Eq. (19). From 3600 to 5400 s, P_{SO} is similar to the value set at the beginning of the simulation. However, this time the battery is charged and discharged more often because it coincides with periods where P_{SO} is either higher or lower than P_{PV}. From 5400 s onwards, it can be observed that the battery reaches and does not exceed the SOC limits.

Fig. 12b illustrates the battery SOC. It can be noted at 6300 s that, when the SOC reaches 90%, the battery is not allowed to charge beyond this point. On the other hand, when the battery SOC reaches 30% at 7100 s, a deeper discharge is not allowed. Moreover, it can be observed that, when the SO does not require a specific power, the battery is discharged during the PP, and charged during the VP. This behavior proves that the EMS avoids exceeding SOC limits, thus increasing the battery life cycle, while making an economic profit out of the smart energy dispatch implemented.

5.5. Comparison of the computational efforts of the models

Due to the simplifications applied to the DM to obtain the SM, the latter can be used for long-term simulations. In this sense, Table 2 presents a comparison of the computational efforts experienced for simulations using the DM and the SM. In Table 2, the simulation horizon represents the simulation time set on Simulink, whereas the second column shows the simulation time reduction of the SM compared to the DM. The computer used for the simulations is equipped with an Intel® Core™ i7-10510U CPU @ 2.3 GHz processor, and 32 GB of RAM. In this case, the PV power plant is simulated as in Case 2, but without any changes in the reactive power reference or voltage sags. Furthermore, the irradiation is assumed constant at 1000 W/m^2, and P_{SO} equals 190 kW, where the PV system provides 171 kW and the battery 19 kW.

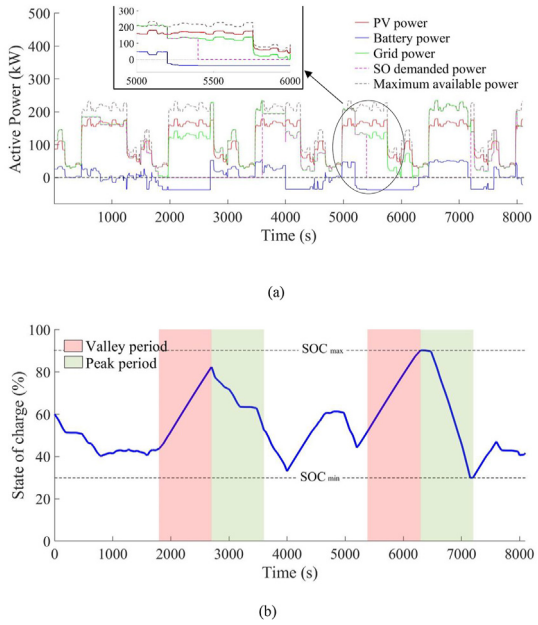

Fig. 12. Case 3: (a) PV power, battery power, grid power, SO demand, and maximum available power; and (b) battery SOC and trading in electricity market.

Table 2
Comparison of the computational effort of the models.

Simulation horizon (s)	SM vs DM Time reduction (%)
5	81%
10	85%
15	86%
20	86%
30	86%
8100	85%
Average time reduction	85%

The results show a 85% time reduction with the SM compared to the DM.

6. Conclusions

This paper presented a new SM of BES-qZSI in large-scale PV power plant, which was evaluated by comparison with the DM (including the modelling of all switches and switching pulses), and the MM implemented exclusively for comparison purposes. The proposed SM was developed through controlled voltage and current sources at the AC and DC side, respectively, so that it can be easily implemented in an electric circuit representation for integration of BES-qZSI into electric power system simulation and modelling software. The control applied to obtain *M* in the SM was the same as in the DM, while *D* was calculated through the battery control that regulated the battery power generation. An EMS was designed to define the battery power reference depending on the PV generation, the power requirements of the SO, the electricity market, and the battery SOC.

The SM, when compared to the DM, obtained similar responses for dynamic events such as fluctuations in the solar irradiation, changes in the electricity market conditions and variable reactive power reference, proving the effectiveness of the proposed SM. Only slight differences appeared in the transitory recovery after the grid fault, but these differences were small enough to be neglected in the target simulations of the SM. Furthermore, when compared to the MM, both models matched almost exactly most of the time, which indicates that the SM reproduces the DC dynamics of the qZSI satisfactorily. Additionally, an experimental HIL setup was built to validate the adequate performance of the SM under different scenarios when compared to the DM.

A great reduction in the simulation time (average time reduction of 85% compared to the DM) and the computational effort was achieved with the SM, making it suitable for long-term simulations, large-scale electric power systems, and control design and dynamic analysis purposes.

Credit author statement

Lais de Oliveira-Assis: Conceptualization, Formal analysis, Investigation, Methodology, Software, Validation, Writing – original draft. **Emanuel P. P. Soares-Ramos**: Conceptualization, Formal analysis, Investigation, Methodology, Software, Validation, Writing – original draft. **Raúl Sarrias-Mena**: Conceptualization, Formal analysis, Investigation, Methodology, Writing – original draft. **Pablo García Triviño**: Conceptualization, Formal analysis, Investigation, Methodology, Writing – original draft. **Enrique González-Rivera**: Methodology, Software, Validation, Writing – review & editing. **Higinio Sánchez-Sainz**: Conceptualization, Formal analysis, Methodology, Writing – review & editing. **Francisco Llorens-Iborra**: Conceptualization, Formal analysis, Methodology, Writing – review & editing. **Luis M. Fernández-Ramírez**: Conceptualization, Funding acquisition, Methodology, Project administration, Supervision, Writing – review & editing.

Declaration of competing interest

The authors declare that they have no known competing financial interests or personal relationships that could have appeared to influence the work reported in this paper.

Acknowledgments

This work was partially supported by the Spain's Ministerio de Ciencia, Innovación y Universidades (MCIU), Agencia Estatal de Investigación (AEI), and Fondo Europeo de Desarrollo Regional (FEDER) Unión Europea (UE) (grant number RTI2018-095720-B-C32), by the Federal Center for Technological Education of Minas Gerais, Brazil (process number 23062–010087/2017-51) and by the National Council of Technological and Scientific Development (CNPq-Brazil).

References

[1] Cabrera-Tobar A, Bullich-Massagué E, Aragüés-Peñalba M, Gomis-Bellmunt O. Topologies for large scale photovoltaic power plants. Renew Sustain Energy Rev 2016;59:309–19. https://doi.org/10.1016/j.rser.2015.12.362.
[2] Sheik Mohammed S, Devaraj D, Imthias Ahamed TP. A novel hybrid maximum power point tracking technique using perturb & observe algorithm and learning automata for solar PV system. Energy 2016;112:1096–106. https://doi.org/10.1016/j.energy.2016.07.024.
[3] Mao M, Zhang L, Duan P, Duan Q, Yang M. Grid-connected modular PV-Converter system with shuffled frog leaping algorithm based DMPPT controller. Energy 2018;143:181–90. https://doi.org/10.1016/j.energy.2017.10.099.
[4] L. Barelli et al., "Comparative analysis of AC and DC bus configurations for flywheel-battery HESS integration in residential micro-grids," Energy, vol. 204, 2020, doi: 10.1016/j.energy.2020.117939.
[5] Pires VF, Romero-cadaval E, Vinnikov D, Roasto I, Martins JF. Power converter interfaces for electrochemical energy storage systems – a review. Energy Convers Manag 2014;86:453–75. https://doi.org/10.1016/j.enconman.2014.05.003.
[6] Periyanayagam M, Suresh Kumar V, Chokkalingam B, Padmanaban S, Mihet-Popa L, Adedayo Y. A modified high voltage gain quasi-impedance source coupled inductor multilevel inverter for photovoltaic application. Energies 2020;13(4). https://doi.org/10.3390/en13040874.
[7] Yuan J, Yang Y, Blaabjerg F. A switched quasi-Z-source inverter with

continuous input currents. Energies 2020;16(3). https://doi.org/10.3390/en13061390.
[8] Ge B, et al. An energy-stored quasi-Z-source inverter for application to photovoltaic power system. IEEE Trans Ind Electron 2013;60(10):4468–81. https://doi.org/10.1109/TIE.2012.2217711.
[9] Grgi I, Basic M, Vukadinovic D. Optimization of electricity production in a grid-tied solar power system with a three-phase quasi-Z-source inverter. J Clean Prod 2019;221:656–66. https://doi.org/10.1016/j.jclepro.2019.02.245.
[10] Ghaderi D, Padmanaban S, Maroti PK, Papari B, Holm-nielsen JB. Design and implementation of an improved sinusoidal controller for a two-phase enhanced impedance source boost. Comput Electr Eng 2020;83. https://doi.org/10.1016/j.compeleceng.2020.106575. 106575.
[11] Liu Y, Ge B, Abu-Rub H, Peng FZ. Overview of space vector modulations for three-phase Z-Source/quasi-z- source inverters. IEEE Trans Power Electron 2014;29(4):2098–108.
[12] Yilmaz AR, Erkmen B. FPGA-based space vector PWM and closed loop controllers design for the Z source inverter. IEEE Access 2019;7:130865–73. https://doi.org/10.1109/ACCESS.2019.2940670.
[13] Mosa M, Balog RS, Abu-Rub H. High-performance predictive control of quasi-impedance source inverter. IEEE Trans Power Electron 2017;32(4):3251–62. https://doi.org/10.1109/TPEL.2016.2531989.
[14] Li Y, Peng FZ, Cintron-rivera JG, Jiang S. Controller design for quasi-Z-source inverter in photovoltaic systems. In: 2010 IEEE energy Convers. Congr. Expo.; 2010. p. 3187–94. https://doi.org/10.1109/ECCE.2010.5618288.
[15] Rajesh R, Mabel MC. A comprehensive review of photovoltaic systems. Renew Sustain Energy Rev 2015;51:231–48. https://doi.org/10.1016/j.rser.2015.06.006.
[16] Reimuth A, Locherer V, Danner M, Mauser W. How do changes in climate and consumption loads affect residential PV coupled battery energy systems? Energy 2020;198:117339. https://doi.org/10.1016/j.energy.2020.117339.
[17] Akbari H, et al. Efficient energy storage technologies for photovoltaic systems. Sol. Energy 2018:1–25. https://doi.org/10.1016/j.solener.2018.03.052. no. March.
[18] van Haaren R, Morjaria M, Fthenakis V. An energy storage algorithm for ramp rate control of utility scale PV (photovoltaics) plants. Energy 2015;91:894–902. https://doi.org/10.1016/j.energy.2015.08.081.
[19] Kamala Devi V, Premkumar K, Bisharathu Beevi A. Energy management using battery intervention power supply integrated with single phase solar roof top installations. Energy 2018;163:229–44. https://doi.org/10.1016/j.energy.2018.08.085.
[20] Angenendt G, Zurmühlen S, Figgener J, Kairies KP, Sauer DU. Providing frequency control reserve with photovoltaic battery energy storage systems and power-to-heat coupling. Energy 2020;194:116923. https://doi.org/10.1016/j.energy.2020.116923.
[21] Chettibi N, Mellit A. Intelligent control strategy for a grid connected PV/SOFC/BESS energy generation system. Energy 2018;147:239–62. https://doi.org/10.1016/j.energy.2018.01.030.
[22] Khajesalehi J, Hamzeh M, Sheshyekani K, Afjei E. Modeling and control of quasi Z-source inverters for parallel operation of battery energy storage systems: application to microgrids. Elec Power Syst Res 2015;125:164–73. https://doi.org/10.1016/j.epsr.2015.04.004.
[23] Khajesalehi J, Sheshyekani K, Hamzeh M, Afjei E. High-performance hybrid photovoltaic -battery system based on quasi-Z-source inverter: application in microgrids. IET Gener Transm Distrib 2015;9(10):895–902. https://doi.org/10.1049/iet-gtd.2014.0336.
[24] Rahman S, et al. Design and implementation of cascaded multilevel qZSI powered single-phase induction motor for isolated grid water pump application. IEEE Trans Ind Appl 2020;56(2):1907–17. https://doi.org/10.1109/TIA.2019.2959734.
[25] Moslehi M, Madadi H, Ali M. Control of a new stand-alone wind turbine-based variable speed permanent magnet synchronous generator using quasi-Z-source inverter. Elec Power Syst Res 2019;177:106010. https://doi.org/10.1016/j.epsr.2019.106010.
[26] Hu S, Liang Z, Fan D, He X. Hybrid ultracapacitor-battery energy storage system based on quasi-Z-source topology and enhanced frequency dividing coordinated control for EV. IEEE Trans Power Electron 2016;31(11):7598–610. https://doi.org/10.1109/TPEL.2016.2518749.
[27] Sun D, Ge B, Bi D, Peng FZ. Analysis and control of quasi-Z source inverter with battery for grid-connected PV system q. Int J Electr Power Energy Syst 2013;46(2009):234–40. https://doi.org/10.1016/j.ijepes.2012.10.008.
[28] Sun D, Ge B, Liang W, Abu-Rub H, Peng FZ. An energy stored Quasi-Z-Source cascade multilevel inverter-based photovoltaic power generation system. IEEE Trans Ind Electron 2015;62(9):5458–67. https://doi.org/10.1109/TIE.2015.2407853.
[29] Liu Y, Ge B, Abu-Rub H, Peng FZ. Modelling and controller design of quasi-Z-source inverter with battery-based photovoltaic power system. IET Power Electron 2014;7(7):1665–74. https://doi.org/10.1049/iet-pel.2013.0389.
[30] Guichi A, Talha A, Madjid E, Mekhilef S. Energy management and performance evaluation of grid connected PV- battery hybrid system with inherent control scheme. Sustain. Cities Soc. 2018;41(May):490–504. https://doi.org/10.1016/j.scs.2018.05.026.
[31] Georgiou GS, Christodoulides P, Kalogirou SA. Optimizing the energy storage schedule of a battery in a PV grid-connected nZEB using linear programming. Energy 2020;208:118177. https://doi.org/10.1016/j.energy.2020.118177.
[32] Corporation SunPower. "X-Series Residential Solar Panels s | X21-335-BLK | X21-345," *sunpower coorporation*. 2016. https://us.sunpower.com/sites/sunpower/files/media-library/data-sheets/ds-x21-series-335-345-residential-solar-panels.pdf.
[33] Liu Y, Abu-Rub H, Ge B, Blaabjerg F, Ellabban O, Loh PC. Impedance source power Electronic converters. Wiley-IEEE Press; 2016.
[34] Liserre M, Blaabjerg F, Hansen S. Design and control of an LCL -Filter-Based three-phase Active rectifier. IEEE Trans Ind Appl 2005;41(5):1281–91.
[35] de Oliveira-Assis L, Soares-Ramos EPP, Sarrias-Mena R, Garcia-Trivino P, Fernandez-Ramirez LM. Large-scale grid connected quasi-Z-source inverter-based PV power plant. In: 2020 IEEE International Conference on Environment and electrical Engineering and 2020 IEEE Industrial and Commercial power systems Europe. EEEIC/I&CPS Europe; 2020. p. 1–6. https://doi.org/10.1109/EEEIC/ICPSEurope49358.2020.9160529. no. 23062.
[36] Fang Zheng Peng. Z-source inverter. IEEE Trans Ind Appl 2003;39(2):504–10. https://doi.org/10.1109/TIA.2003.808920.
[37] Yazdani A, Iravani R. Voltage-sourced converters in power systems: Modeling, control, and applications. Wiley-IEEE Press; 2010.
[38] P. García, J. P. Torreglosa, L. M. Fernández, and F. Jurado, "Improving long-term operation of power sources in off-grid hybrid systems based on renewable energy, hydrogen and battery," J Power Sources, vol. 265, pp. 149–159, Nov. 2014, doi: 10.1016/j.jpowsour.2014.04.118.